Schweizerischer Erdbebendienst
Service Sismologique Suisse
Servizio Sismico Svizzero
Swiss Seismological Service

ETH zürich

SITE CHARACTERIZATION REPORT
SUSI: Lugano (TI), Università della Svizzera Italiana

Paolo Bergamo, Francesco Panzera, Donat Fäh

Last modification: 31.03.2020

Schweizerischer Erdbebendienst (SED)
Service Sismologique Suisse
Servizio Sismologico Svizzero
Servizi da Terratrembels Svizzer

ETH Zurich
Sonnegstrasse 5
8092 Zuerich
Schweiz
paolo.bergamo@sed.ethz.ch

Contents

Summary

The SSMNet station SUSI was installed on 25.07.2017 in the city center of Lugano (TI), in the green area in front of the main entrance of the Università della Svizzera Italiana (USI). SUSI is located approximately in the middle of the basin hosting the city of Lugano; the basin stretches along a north-south axis and opens up at its southern end to the Lake of Lugano. The basin is constituted by alluvial sediments of the Holocene period.

The characterization of the site was ensured by a microtremor measurement performed with an array of 13 stations deployed over a circular area having a diameter of 300 m, approximately centered at SUSI.

The site is characterized by a low fundamental frequency (0.9 Hz), which is associated to a 2D SH resonance phenomenon induced by the geometry of the sedimentary basin.

The obtained velocity model is the following: the shallowest 40-50 meters have an S-wave velocity around 350 m/s and they are likely to be constituted by alluvial sediments. Below, V_S gradually increases until reaching about 650 m/s at ~150 m depth; this depth range might be occupied by sediments more compacted by self-weight, or moraine (which borders the basin where SUSI is located). The bedrock is met at approximately 150 m depth, and it has a V_S of about 1000 m/s (weathered rock). The obtained velocity profiles show a further increase in S-wave velocity at about 250 m depth, suggesting a transition between weathered to fresh rock below; however, this interface lies at the lower boundary of the investigation depth, so it must be accepted with a certain level of uncertainty.

The obtained V_{S30} is 328 m/s (standard deviation 18 m/s); H_{800} (depth where V_S exceeds 800 m/s) is 154 m (standard deviation = 22 m); therefore, the site can be classified as type C according to both Eurocode 8 (CEN, 2004) and SIA261 (SIA, 2014).

1. Introduction

In the framework of the second phase of the SSMNet (Swiss Strong Motion Network) renewal project, a new station, labelled as SUSI was installed in the city centre of Lugano, in a green area in front of the main entrance of the Università della Svizzera Italiana (Figure 1); the station started recording on 25th July 2017. SUSI is located approximately along the centerline of the basin hosting the main part of Lugano; the basin stretches along a north-south axis and it opens up southwards to the Lake of Lugano. At the location of SUSI this basin is circa 1300 m wide, and it is constituted by alluvial sediments of the Holocene period.
The characterization of the site was ensured by a microtremor measurement performed with an array of 13 stations deployed over a circular area having a diameter of 300 m, approximately centered at SUSI.

2. Geological setting

The basin hosting the center of Lugano stretches along a north-south axis and opens up to the south to the Lake of Lugano. At the location of SUSI, the basin is approximately 1300 m wide, and it is constituted by alluvial sediments of the Holocene period. The basin is bordered to the west and east by elevations of moraine (till), encasing outcrops of the underlying paragneiss. To the north-east of SUSI, an alluvial fan of ~1000 m width is present.

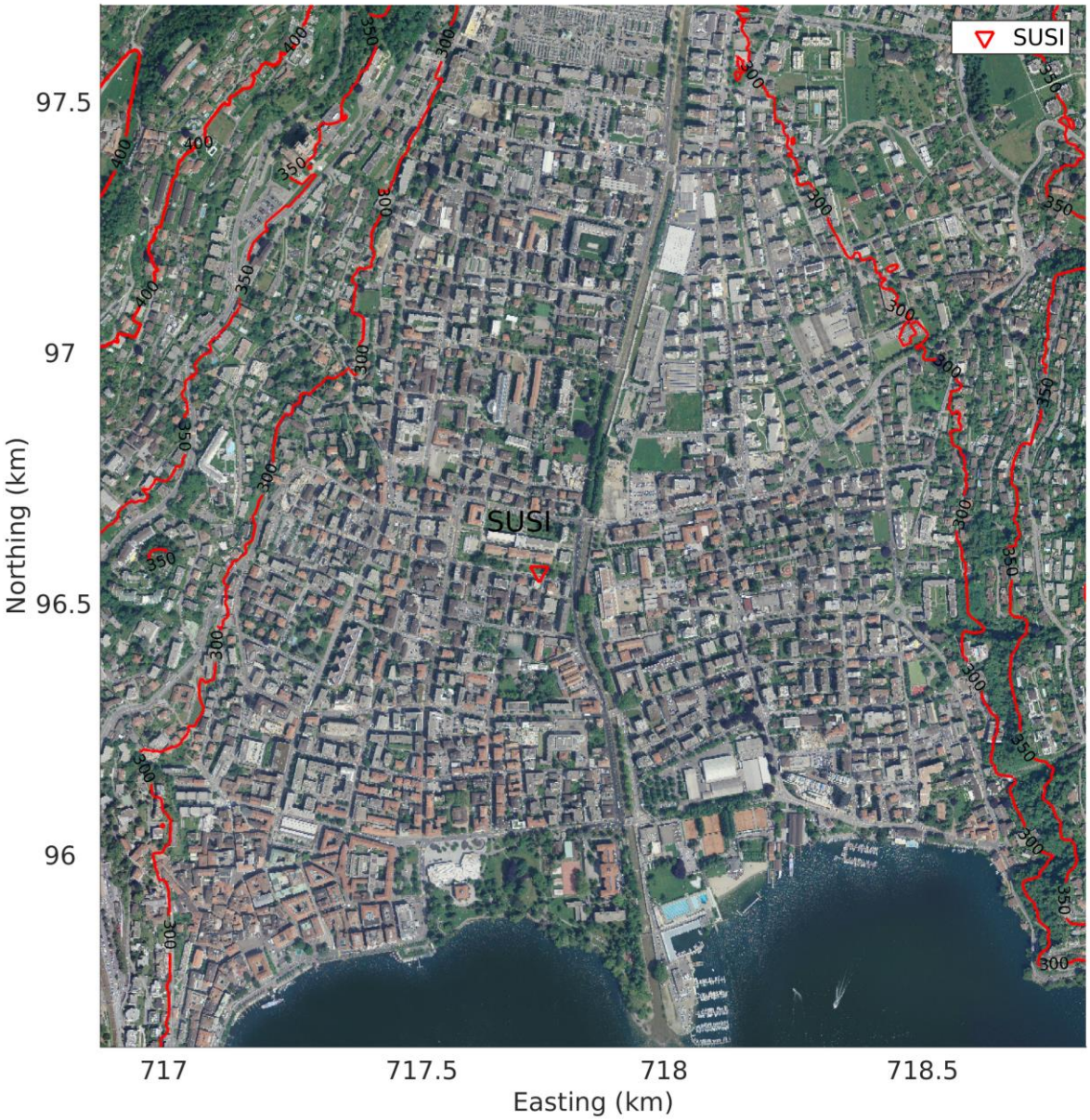

Figure 1 – geographical location of SUSI (red trangle) in the city center of Lugano. Red contour lines represent the elevation. The contour interval is 50 meters (© Swisstopo).

Figure 2 – Location of SUSI (red trangle) on the 1:25000 geological atlas (sheet LK 1353, Swisstopo 1976). The central part of the basin hosting the city of Lugano is constituted by alluvial sediments of the Holocene period (light blue); the basin is bordered to the east and west by moraine (till) of the late Pleistocene (light green), encasing some areas of outcropping Paragneiss (brown). To the north-east an alluvial fan is present (white).

3. Seismic acquisition

The site characterization of SUSI was performed with a passive array measurement, carried out on 09.11.2017. Figure 3 shows the geometry of the recording array, constituted by 13 stations.

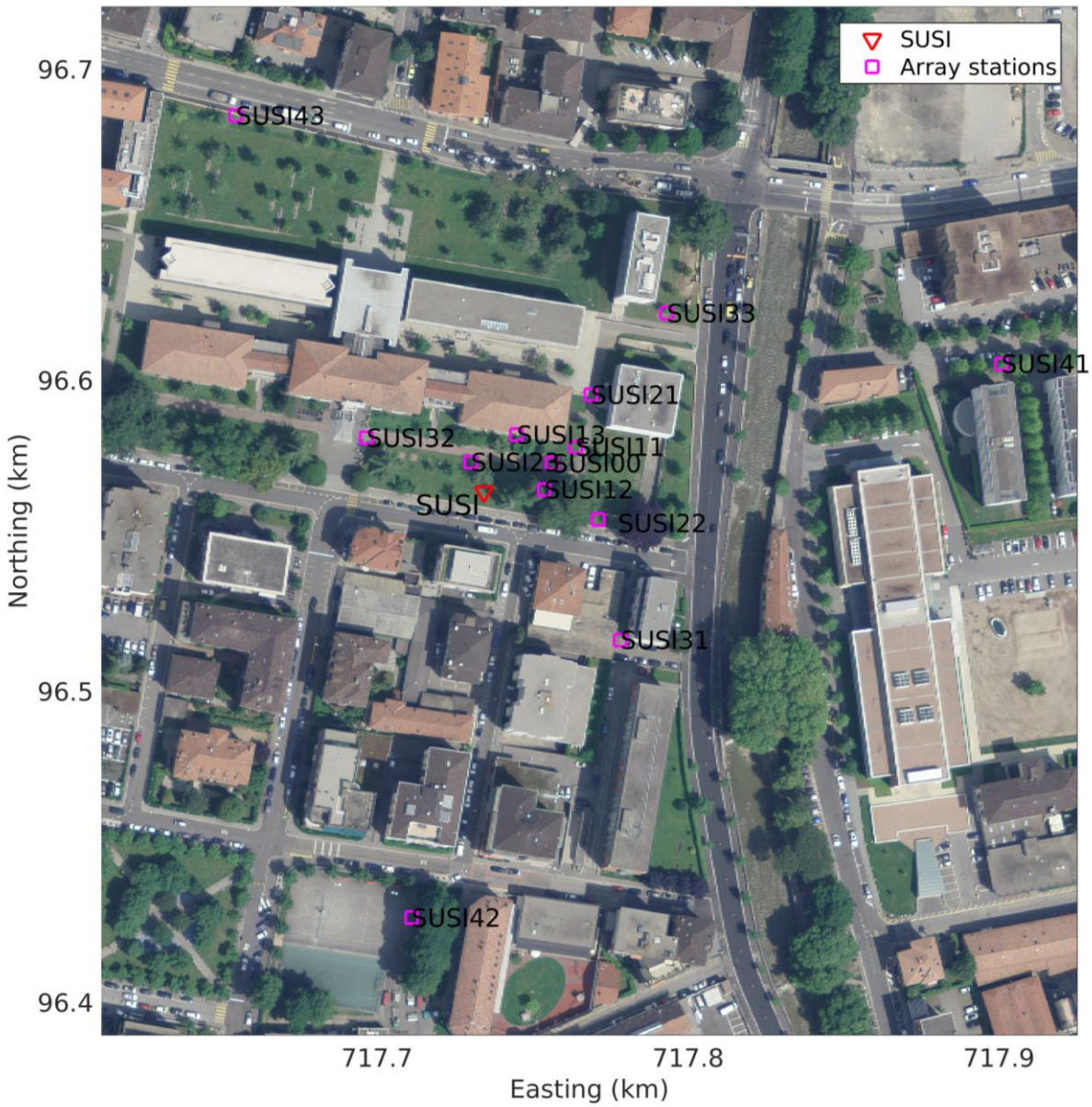

Figure 3 – Position of the passive array. Magenta squares: stations of passive array (with corresponding name); red triangle: permanent station SUSI.

3.1 Passive seismic measurement

The passive seismic array was installed in the urban area of Lugano, approximately centered at stations SUSI. It consisted of 13 seismic sensors (see Fig. 3), deployed along 4 concentric circles having their center in the station SUSI00. The radii of the circles were 9.6, 24, 60 and 150 m, i.e. increasing on a logarithmic scale. Along each circle 3 stations were positioned at the corners of an equilateral triangle, rotated by 35 degrees with respect to the triangle of the inner circle. The result is a spiral-shaped array; small modifications from this regular plan were put in place on the ground to adapt to the locations of buildings and roads. The maximum interstation distance was 264 m, the minimum 8.8 m, the median 76.8 m.

The 13 stations consisted of three-component Lennartz 5s sensors, which had been connected to a total of 12 Quanterra Q330 digitizers; at the center of the array, two sensors were connected to the

same digitizer. The sampling frequency was 200 Hz; the recording lasted from 14:20 to 17:45 (local time). The stations were installed on metal tripod. Whenever possible, a small hole ~20 cm deep was dug into the soil to house the tripod and the sensor, for better coupling; alternatively, the tripod was placed directly on the asphalt surface (Figure 4).
The station locations were measured by a differential GPS system (Leica Viva GS10), which was set up to measure with a precision better than 5 cm.

Figure 4 – Examples of station installation. Left: the tripod and the sensor are housed into a small hole dug into the soil. Right: the tripod is directly placed on cobbles.

4. Data processing

Data acquired in the passive survey was processed in order to determine the characteristics of propagation of surface waves (Rayleigh and Love), as well as the resonance frequency of the site.

4.1 Passive data processing

4.1.1 H/V analysis

The seismic data (three component traces) acquired by each sensor of the passive array were processed with:

- classical H/V techniques (as implemented in the Geopsy software, www.geopsy.org; classical H/V of Fäh et al., 2001), determining the spectral ratio between horizontal and vertical components, whose peaks are related to the frequencies of resonance of the site;
- more refined algorithms, estimating the ellipticity of Rayleigh wave as a function of frequency (Raydec, Hobiger at al., 2009; time-frequency method, Poggi and Fäh, 2010; wavelet-based time-frequency method as implemented in the Geopsy software). These methods aim at eliminating the contributions of other waves besides Rayleigh waves, to obtain a more reliable estimation of Rayleigh wave ellipticity when compared to the classical H/V technique.

Fig. 5 collects all the H/V curves from the sensors of the array, obtained applying the time-frequency method of Poggi and Fäh (2010). Most of the curves exhibit a similar appearance in the frequency band 0.4 – 5 Hz, with a broad hump between 0.4 – 2 Hz having its peak at 0.8 – 1 Hz (identified as fundamental frequency). The general consistency of the H/V curves suggests a relatively 1D configuration for the subsurface beneath the array. The only (partial) exception to the overall trend is constituted by the curve of station SUSI43, in the north-western corner of the array (Figure 3). The hump between 0.4 – 2 Hz is in fact quite flat. A possible explanation for this anomaly is the location of SUSI43, just beside a heavily congested road; the traffic might have excessively influenced the recorded wavefield.

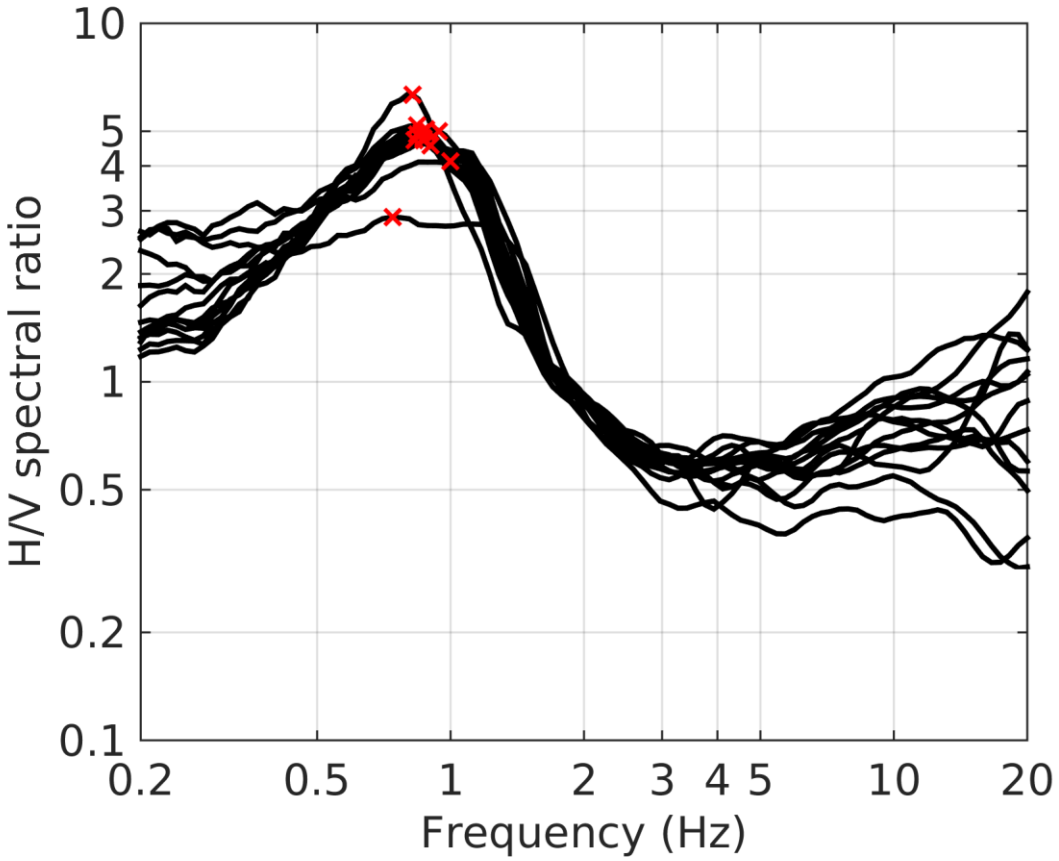

Figure 5 – H/V curves (obtained using the time-frequency method of Poggi and Fäh, 2010) from the stations of the array. Red crosses mark the picked fundamental frequency.

Fig. 6 displays some sample H/V curves, as well as the spatial distribution of the picked fundamental frequencies. It is possible to observe that, from south-east to north-west, the left flank of the main peak broadens. As for the f_0 values, they do not show a significant variability, as most

of them are comprised within 0.82 – 0.94 Hz; the only two outliers are the f_0s referring to SUSI43 (0.74 Hz) and SUSI32 (1 Hz), both located north-west of the array center (Figure 3), whose H/V curves show a broad hump which may have hampered the identification of the peak.

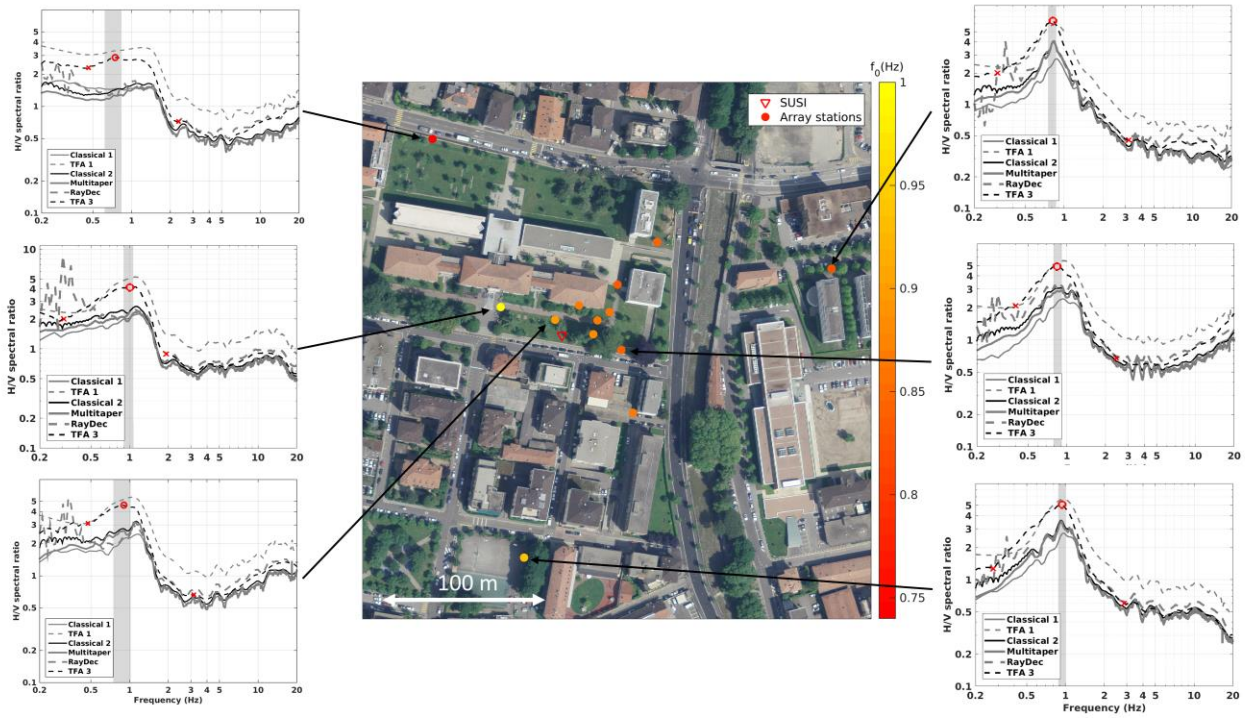

Figure 6 – H/V curves from selected passive array stations, obtained using different methods (Classical 1: Geopsy; Classical 2: Fäh et al., 2001; TFA1: wavelet-based time-frequency method as implemented in Geopsy software; TFA3: time-frequency method, Poggi and Fäh, 2010). The location of all stations is indicated by a dot whose color scales with the value of the corresponding f_0.

4.1.2 RayDec

The RayDec technique (Hobiger et al., 2009) is supposed to eliminate the contributions of other wave types than Rayleigh waves and give a better estimate of the ellipticity than the classical H/V technique. The results of this processing are shown in Fig. 7 and are similar to the H/V curves. The curves show a good consistency. Below 0.5 Hz, the ellipticity curves are quite high and do not seem to be realistic. Between 0.5 and 2 Hz, the curves draw a broad peak, with the right flank steeper than the left one. Above 5 Hz, the curves show more variability, probably caused by shallow heterogeneities.

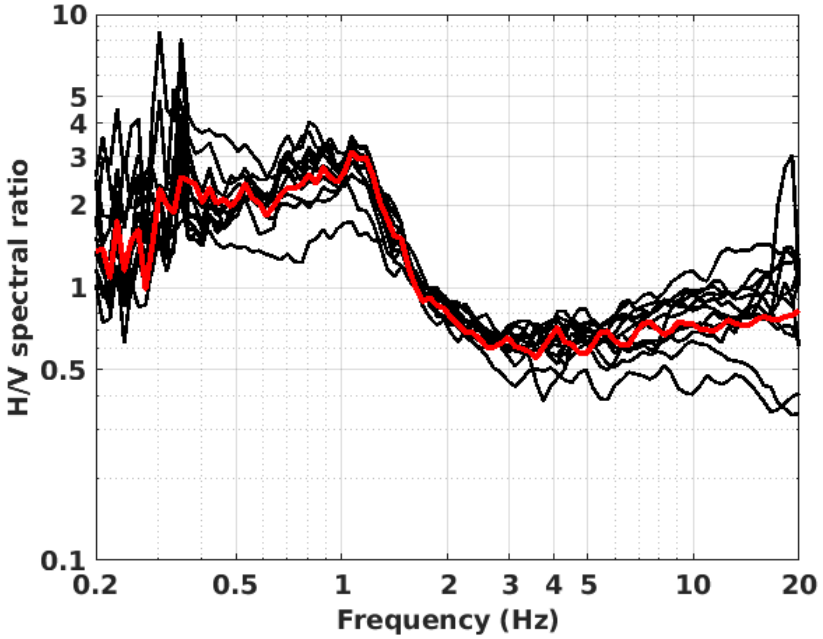

Figure 7 – Rayleigh wave ellipticity curves determined using RayDec for all the stations of the array. The curve in red refers to the central station (SUSI00).

4.1.3 Polarization analysis

Considering the geomorphology of the site (basin), a polarization analysis on the array data was performed to check for 2D resonances using the method of Burjánek et al. (2012): the results are represented in Figs. 8 and 9.

We remind that, according to Burjánek et al. (2012) the ellipticity is here (Fig. 8) defined as the ratio between the semi-minor and semi-major axes of the ellipse that describes the particle motion in the 3D Euclidean space for each considered time window and frequency; therefore, the particle motion related to the propagation of Rayleigh waves should be indeed characterized by low values of ellipticity, at the frequencies with prevalent horizontal motion. Additionally, troughs in the ellipticity graphs are also caused by 2D/3D resonance phenomena and preferential directions of noise wave-field.

In our case, a match between peaks in H/V curves (Fig. 6) and marked troughs in ellipticity graphs (Fig. 8), can be established for the 0.8 – 1 Hz frequency band. More interestingly, the polar-strike plots (Figure 9) indicate significant directional effects in the direction NW-SE at the resonance frequency (f_0) of all stations. This feature is likely to be related to 2D SH resonance phenomena in the basin where SUSI is located (Bard and Bouchon, 1985, Ermert et al., 2014; see discussion in section 6.2).

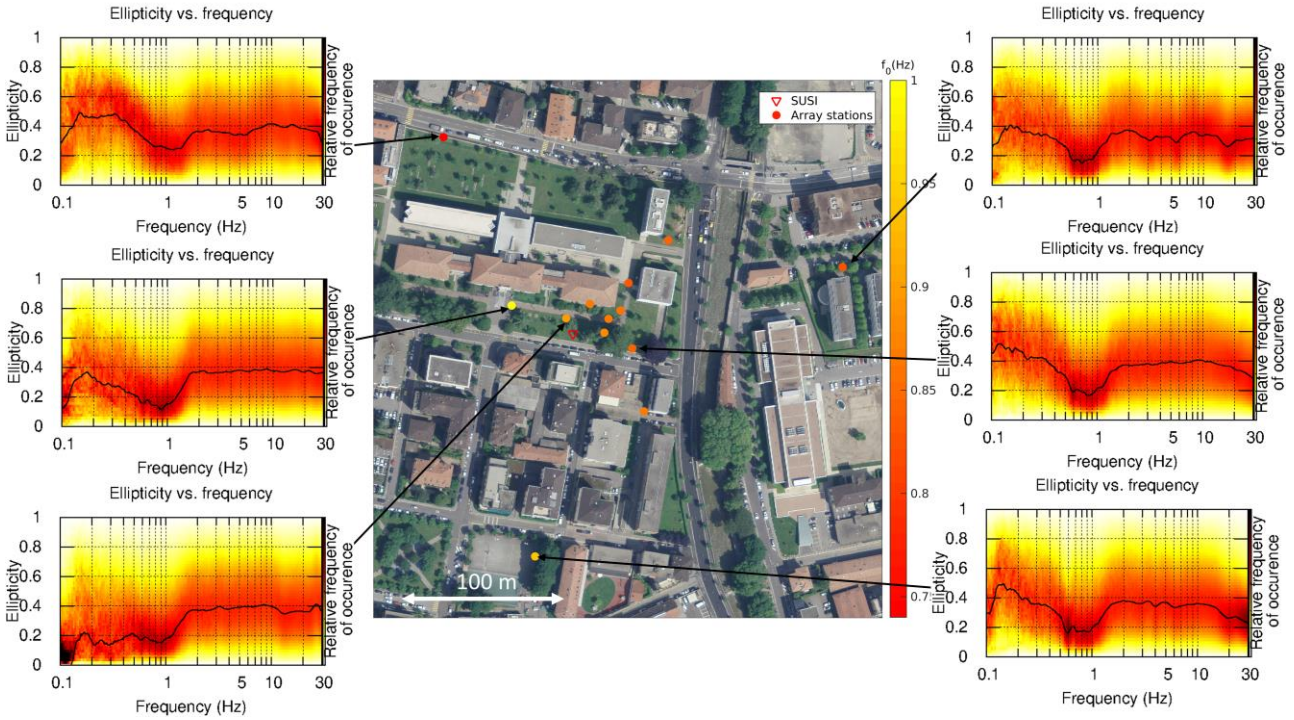

Figure 8 – Polarization analysis. The insets surrounding the map of the passive array contain the ellipticity (as defined in Burjanek et al., 2012) graphs for some sample sensors (same of Figure 6). The location of all stations is indicated by a dot whose color scales with the value of the corresponding f_0.

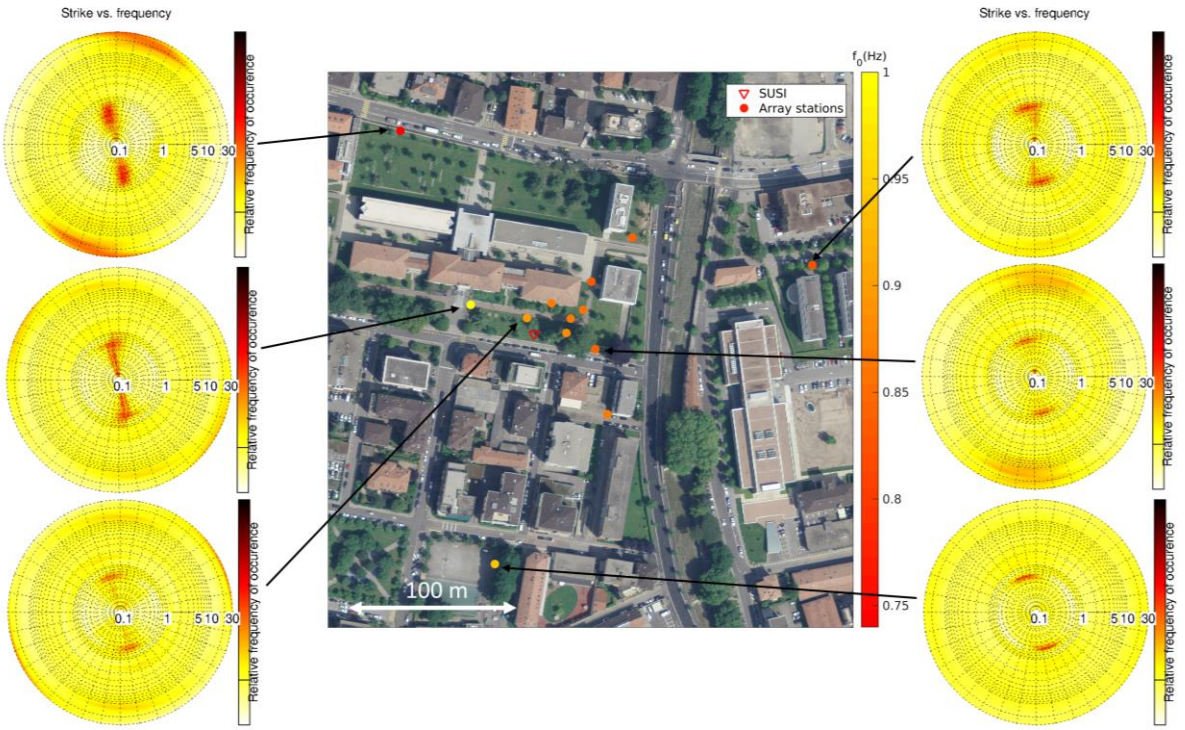

Figure 9 – Polarization analysis. The insets surrounding the map of the passive array contain the polar strike (as defined in Burjanek et al., 2012) graphs for some sample sensors (same of Figure 6). The location of all stations is indicated by a dot whose color scales with the value of the corresponding f_0.

4.1.4 Three-component high-resolution fk

Besides single-station interpretation (see previous subsections), the recordings from the passive array were also jointly processed with the aim of estimating the parameters of propagation (phase velocity, ellipticity, azimuth) of surface (Rayleigh and Love) waves. The used techniques are the three-component high resolution *fk* analysis (HRFK) of Poggi and Fäh (2010), and the wavefield decomposition method implemented in the WaveDec code by Maranò et al. (2012; analysis and results described in the following section).

The results of the high-resolution *fk* analysis are shown in Figs 10 (overall results and picking) and 17 (picked curves). The phase velocity dispersion curves obtained for the vertical and radial components (therefore related to the Rayleigh wave propagation), are mutually consistent in the 3 – 10 Hz frequency band, drawing a continuous branch with velocities gently decreasing from 350 m/s (at 3 Hz) to 290 m/s (10 Hz). Below 3 Hz, the vertical component curve increases its phase velocity to 675 m/s at 1.8 Hz (at the array resolution limit), while the radial component curve shows a steeper velocity increment (775 m/s at 2 Hz), probably due to a jump to the first higher mode. The corresponding Rayleigh wave ellipticity curves are rather flat (just below 1 across the whole frequency band) and do not show marked peaks or troughs.

As for the transversal component (Love waves propagation), the dominant feature is a dispersive branch whose phase velocity gently increases from 350 m/s at 10 Hz to 520 m/s at 1.4 Hz (within the array resolution limits). At high frequency, between 5 – 7 Hz, a second branch, probably related to the 1st higher mode of propagation, can be identified.

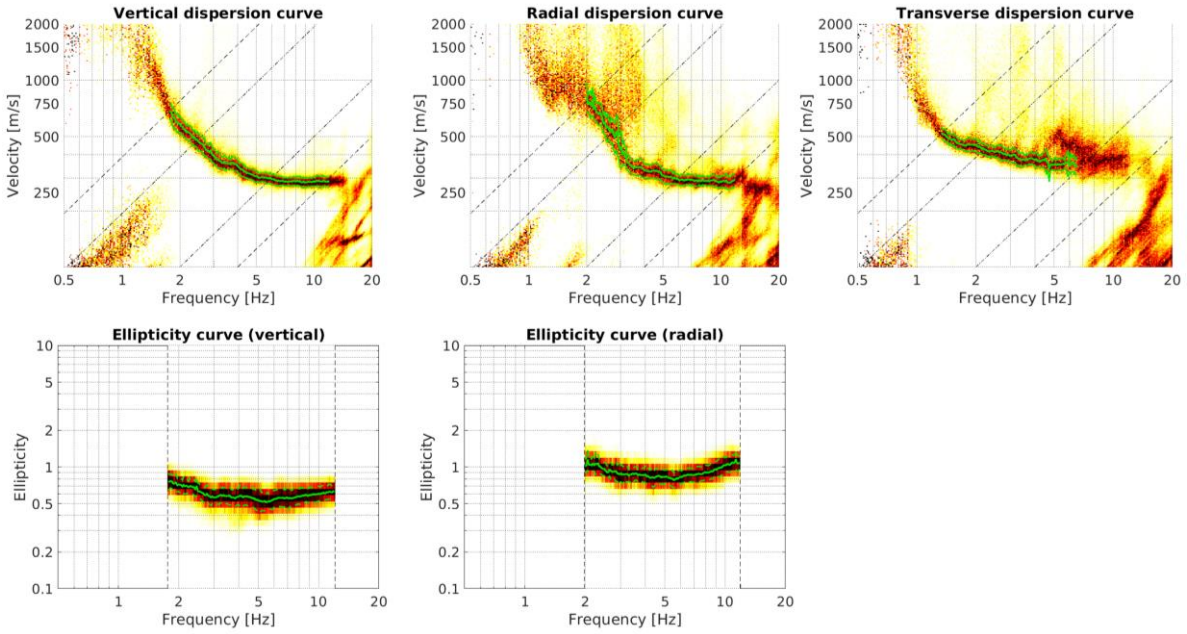

Figure 10 – Three-component high-resolution fk processing results. Top: phase velocity vs frequency graphs obtained from the three components of propagation. Bottom: ellipticity curves obtained from vertical and radial component. Dashed lines indicate the array resolution limits, while green lines indicate the picked curves (central values and standard deviation interval).

4.1.5 Wave field decomposition

The passive seismic data were also processed with the wave field decomposition technique implemented in the WaveDec code by Maranò et al. (2012). The code jointly analyzes all recordings from all sensors and components, estimating the parameters (phase velocity, ellipticity) of Rayleigh and Love wave propagation. The recorded wave field is subdivided into time windows, and each window is decomposed into a number of waves that best explains it; wave propagation parameters are then estimated for each wave with a maximum likelihood approach. The sharpness of the wave property estimation can be modified between purely maximum likelihood estimation and a Bayesian Information Criterion by changing a parameter called γ. Here, a value of $\gamma = 0.2$ was used, corresponding to a mainly maximum likelihood estimation.

The WaveDec results are shown in Figs 11 and 12 (collation with HRFK results). As for Rayleigh waves, the identified curve matches quite well the picking from HRFK, vertical component, drawing a continuous branch – to be identified as fundamental mode – extending across the whole available frequency band, with phase velocities decreasing from 675 (at 1.8 Hz) to 280 m/s (at 10 Hz). The corresponding ellipticity angle curve increases from angle = -0.6 rad at 12 Hz to about 0 rad at 1.7 Hz, indicating a change in the direction of particle motion, from retrograde to prograde (below 1.7 Hz). This zero-crossing of the ellipticity angle corresponds to a singularity in the relevant ellipticity curve (Figure 12, upper right subplot), which does not appear in the results from HRFK analysis.

The Love wave curve matches the corresponding results from HRFK, with a continuous branch stretching across all the available frequency range, with phase velocities decreasing gently from 520 m/s at 1.4 Hz to 350 m/s at 10 Hz.

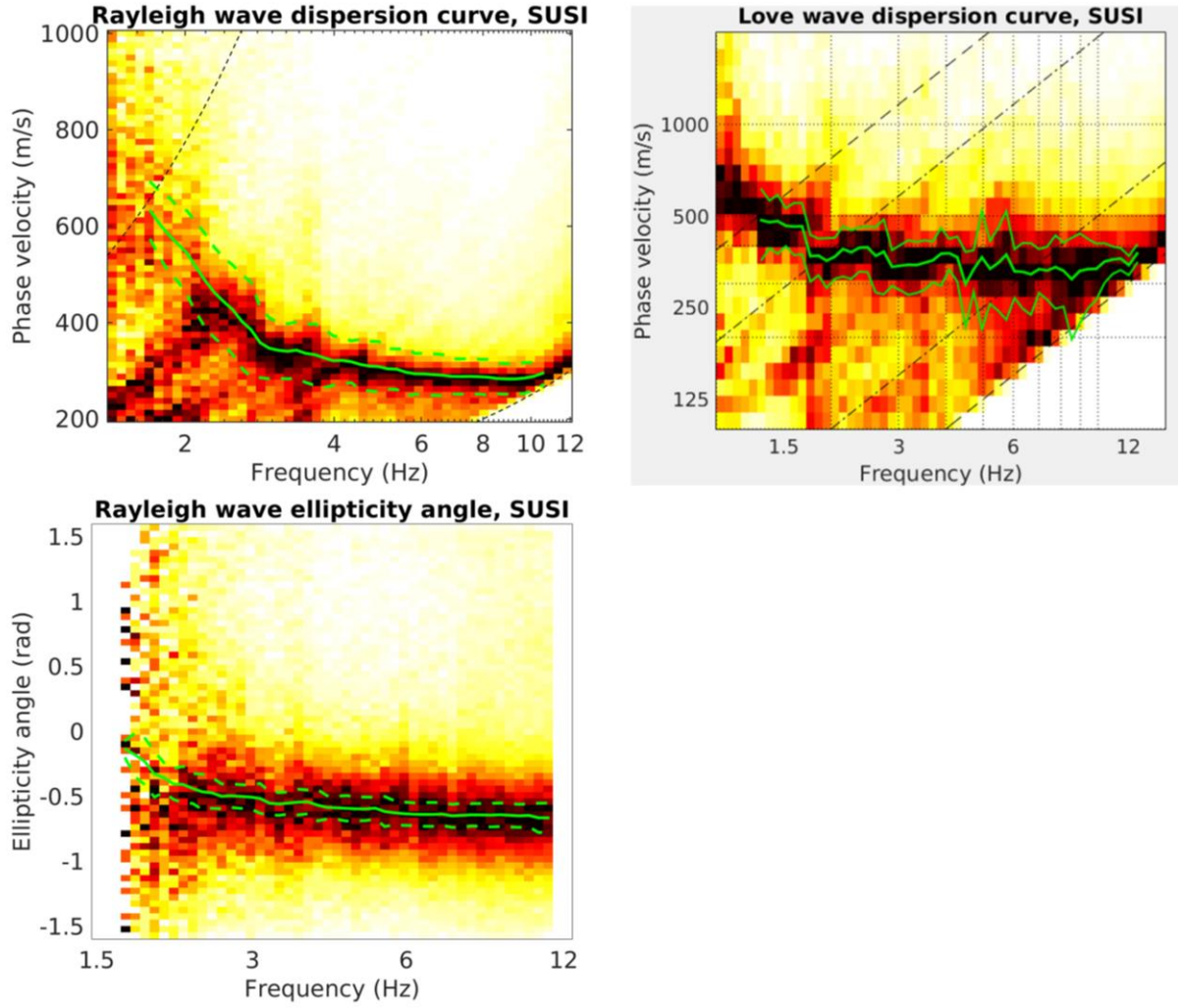

Figure 11 – Love and Rayleigh wave dispersion (top) and ellipticity angle (bottom) curves obtained with the WaveDec technique (Maranò et al., 2012). The dashed black lines indicate the theoretical array resolution limits, the central green line indicates the picked curves, the upper and lower green lines indicate the standard deviation.

4.1.6 Comparison of HRFK and WaveDec results.

The results of the picking operation of the HRFK and WaveDec data are directly collated in Figure 12. As for the Rayleigh wave dispersion curve (upper left subplot), the vertical component HRFK and WaveDec data agree in defining a dispersive branch, identified as fundamental mode, across the whole available frequency band (1.7 – 12 Hz). The radial component HRFK data appear to "jump" at ~ 3 Hz towards the first higher mode, possibly because of a poor energetic content – in this frequency band - of this component on the Rayleigh wave fundamental mode. This is in agreement with the Rayleigh wave fundamental mode ellipticity curve retrieved with WaveDec (upper right panel), which departs - at around 3 Hz – from a ratio ≈ 1 towards a downward singularity at 1.7 Hz, indicating a prevalence of the vertical over the horizontal modal displacements. As for the Love

wave dispersion curve, here again the fundamental modes from HRFK and WaveDec match quite well, drawing a continuous dispersive branch across all the available frequency band.

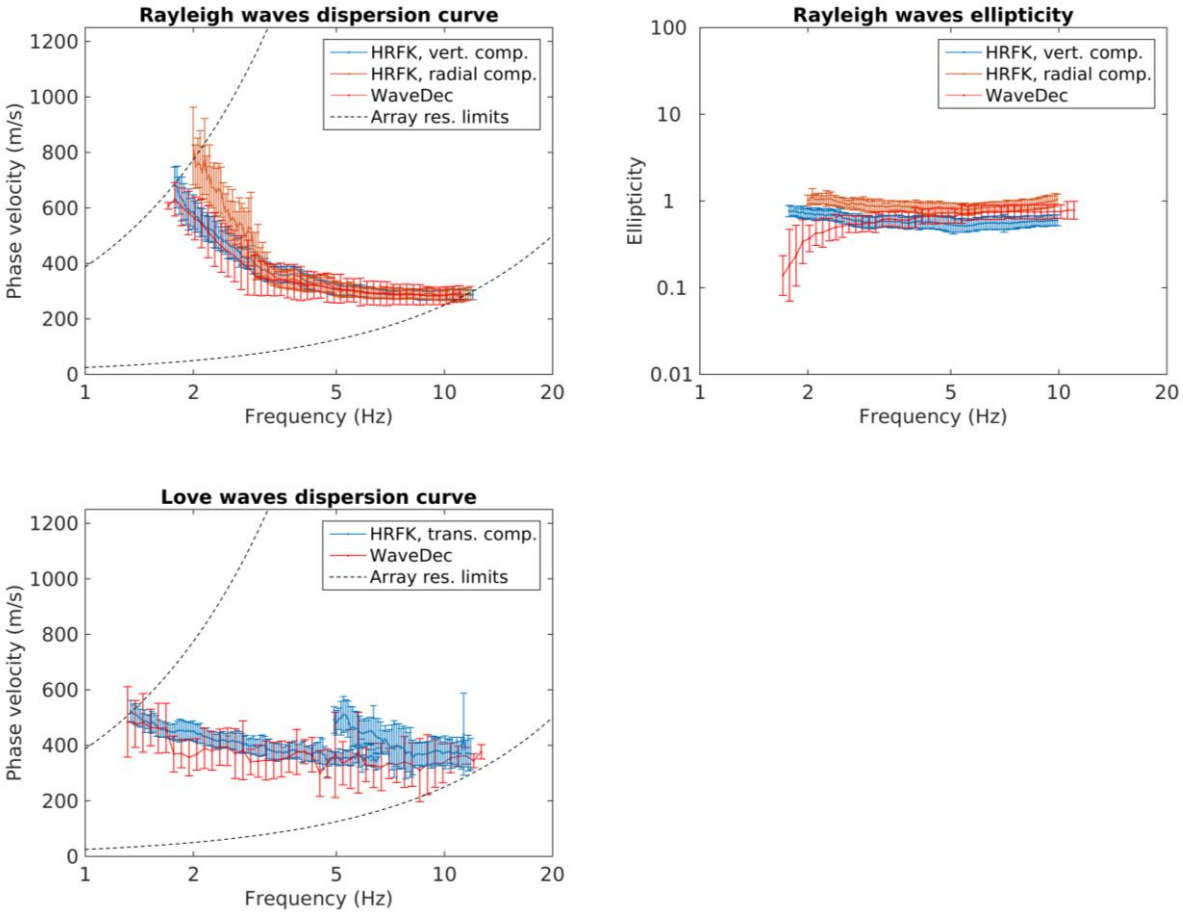

Figure 12 – Comparison of the estimated Rayleigh and Love wave phase velocity curves and the Rayleigh wave ellipticity curves (fundamental mode) from different processing methods of the passive array data.

5 Surface wave data inversion

The retrieved phase velocity dispersion curves of Rayleigh and Love waves as well as the Rayleigh wave ellipticity curve (section 4), were inverted for a 1D profile of the seismic properties of the subsurface. For the inversion an ad-hoc code implemented in Matlab® was used. The code performs a Monte Carlo inversion, first generating a population of possible joint V_S/V_P profiles, then computing the synthetic curves corresponding to each model, and finally evaluating the misfit with respect to the experimental curves. For the solution of the forward problem we resorted to Hermann (2013).

5.1 Inversion target

The inversion target was selected from the results of HRFK and WaveDec processing of passive array data (Figure 12). As for the fundamental mode of Rayleigh waves, we selected the dispersion and ellipticity curve from WaveDec, as the joint processing of radial and vertical components

ensures a greater reliability, particularly for ellipticity information. We did not combine the ellipticity data from the array with those from single-station data processing (Figure 7), as below the array resolution lower threshold (1.7 Hz) the 2D resonance effect becomes significant (Figure 9), hence the latter may affect the Rayleigh wave ellipticity representation from single station data at low frequency. The first higher mode of Rayleigh wave propagation was identified only on the HRFK radial component data, and was added to the inversion target. The Love wave dispersion curve from HRFK (transversal component), was preferred over the corresponding curve from WaveDec, as it shows a better consistency in the phase velocity estimation, particularly at low frequency.

Phase velocity and ellipticity data were resampled on a logarithmically scaled frequency vector, with 100 elements between 1.33 and 12 Hz.

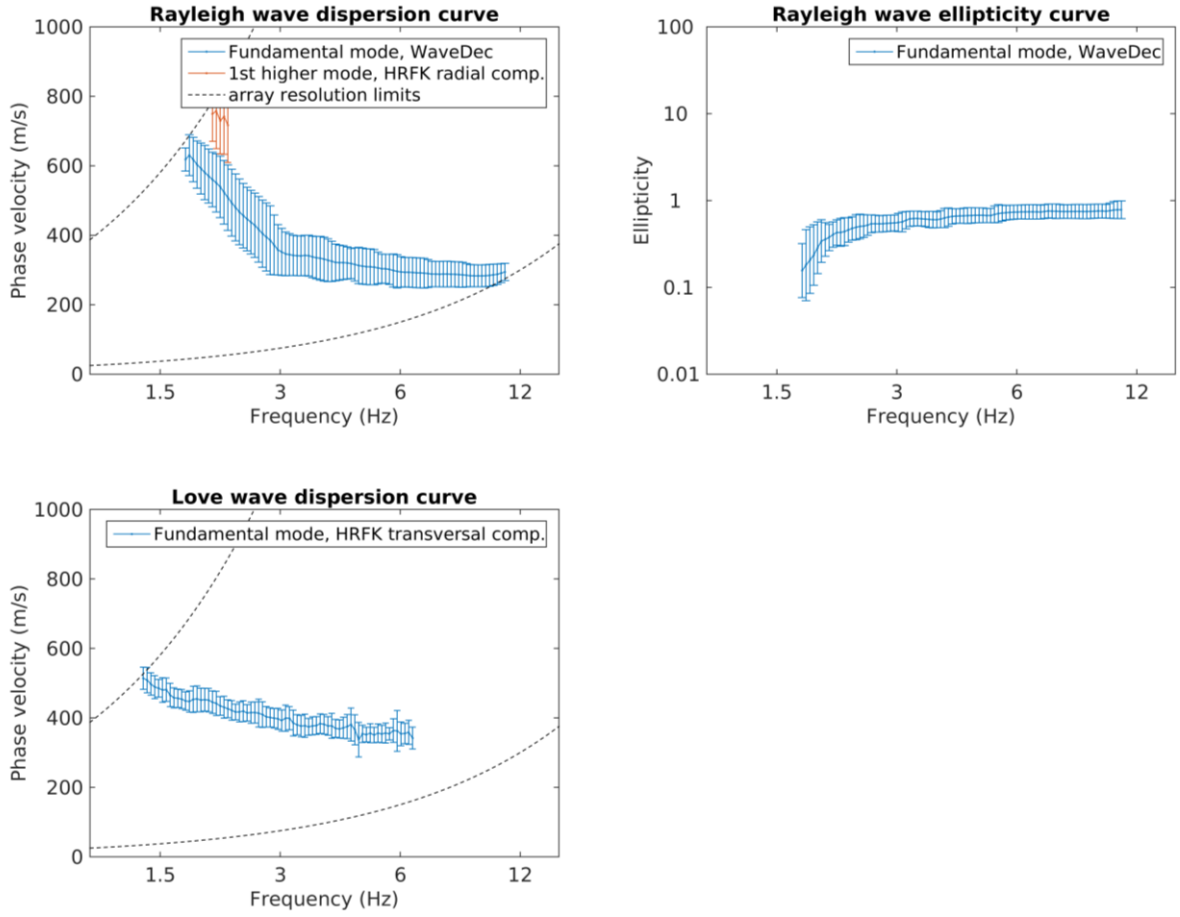

Figure 13 – Inversion target. Rayleigh wave (top left) fundamental and 1st higher mode, and Love wave (bottom left) fundamental mode. Top right: fundamental mode ellipticity curve.

5.2 Parameterization of the model space

After several preliminary attempts, we adopted three different subsurface parameterizations:

1) In the first parameterization, the subsurface was modeled as a stack of 7 homogeneous layers, whose velocity (V_P, V_S) and thickness values were left free to vary within pre-defined ranges.
2) In the second parameterization, the subsurface was modeled as a stack of 6 homogeneous layers, whose velocity (V_P, V_S) and thickness values were left free to vary within pre-defined ranges.
3) In the third parameterization, the subsurface was modeled as a stack of 14 homogeneous layers with fixed thicknesses (increasing with depth), and whose velocity (V_P, V_S) values were left free to vary within pre-defined intervals.

In all parameterizations, density values are attributed a-priori to the layers: values increase with depth and they range from 1900 kg/m^3 (shallowest layer) to 2250 kg/m^3 (half-space). The Poisson's ratio(s) for the layer(s) occupying the shallowest ~10 m was defined as comprised between 0.2 – 0.4, while for the deeper formations the upper limit was extended to 0.49, to allow for the presence of water-saturated layers (consistently with the piezometric information from a nearby NAQUA-QUANT monitoring site, Pregassona – Pozzo Fola, BAFU 2017). The Poisson's ratio interval for the lower halfspace is restricted to 0.2 – 0.35 (values consistent with those of a non-water saturated rock).

For each parameterization, we completed an inversion run with 10^6 randomly generated profiles.

5.3 Inversion results

In the following figures we show the inversion results obtained from the each of the three subsurface parameterizations illustrated above: Figures 14-15 show the 20 best performing models from the 7-layer parameterization inversion, Figures 16-17 refer to the 6-layer parameterization inversion, Figures 18-19 refer to the 14-layer parameterization inversion. The three inversions produce similar best performing V_S profiles: the S-wave velocity is quite low (around 350 m/s) in the shallow 40-50 m, then it increases to ~ 550 m/s in the depth range 50 – 150 m. At the latter depth (150 m), V_S sharply increases to 1000-1500 m/s, then further increments to around 2000 m/s at approximately 250 m depth. The minimum misfit experimental-simulated data is achieved by the 14-layer parameterization (its minimum RMSerror being 0.4, versus 0.5 of 6- and 7-layer parameterizations): the reason is that, thanks to the larger number of layers (particularly at shallow depths), the Rayleigh wave dispersion curve can be better fitted at high frequencies (around 10 Hz). Apart from this detail, the fit of the experimental curves is similar and good for all three parameterizations. As final inversion result, we consider the set of 21 profiles constituted by the 7 best performing models from each of the three inversion runs.

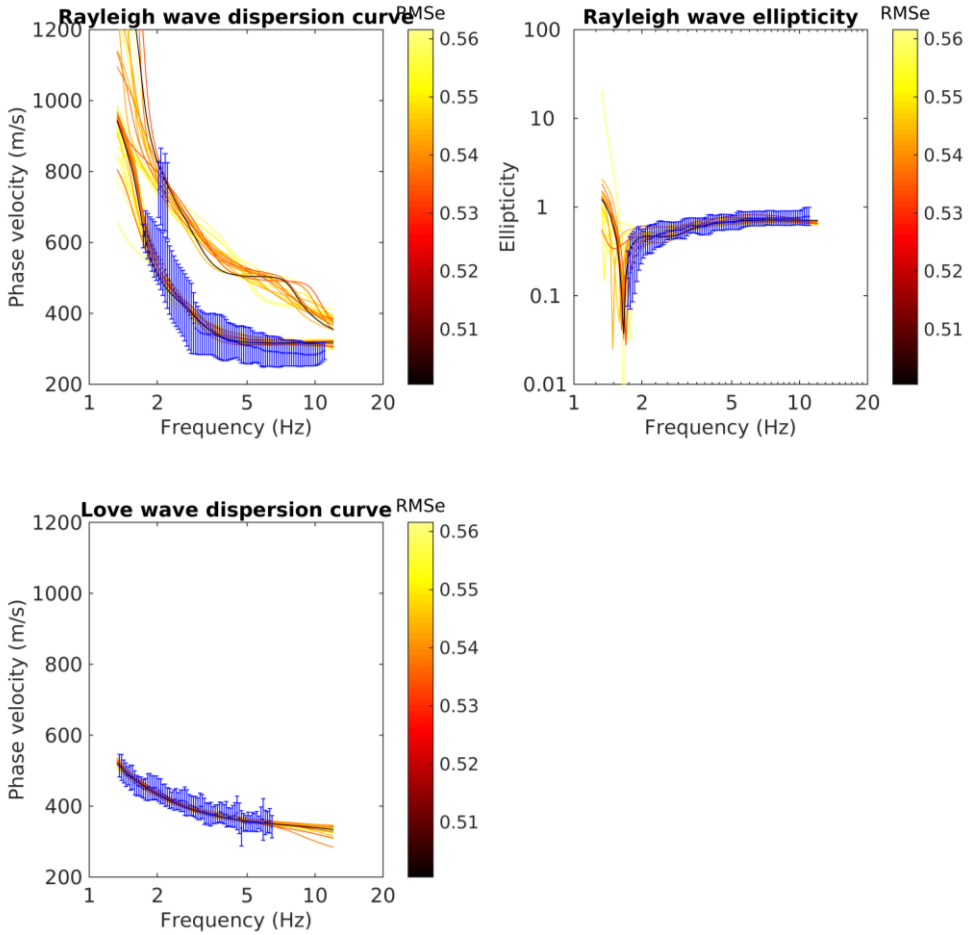

Figure 14 – 7-layer parameterization inversion: fit between experimental data (blue dots with error bars) and synthetic curves (colored lines) for the 20 best performing models.

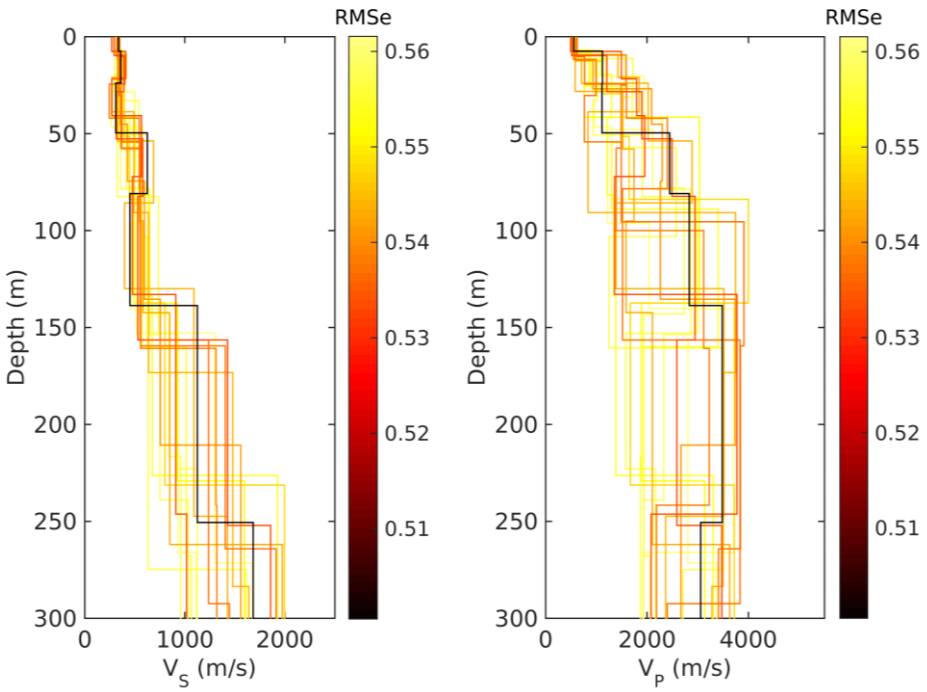

Figure 15 – 7-layer parameterization inversion: 20 best performing models.

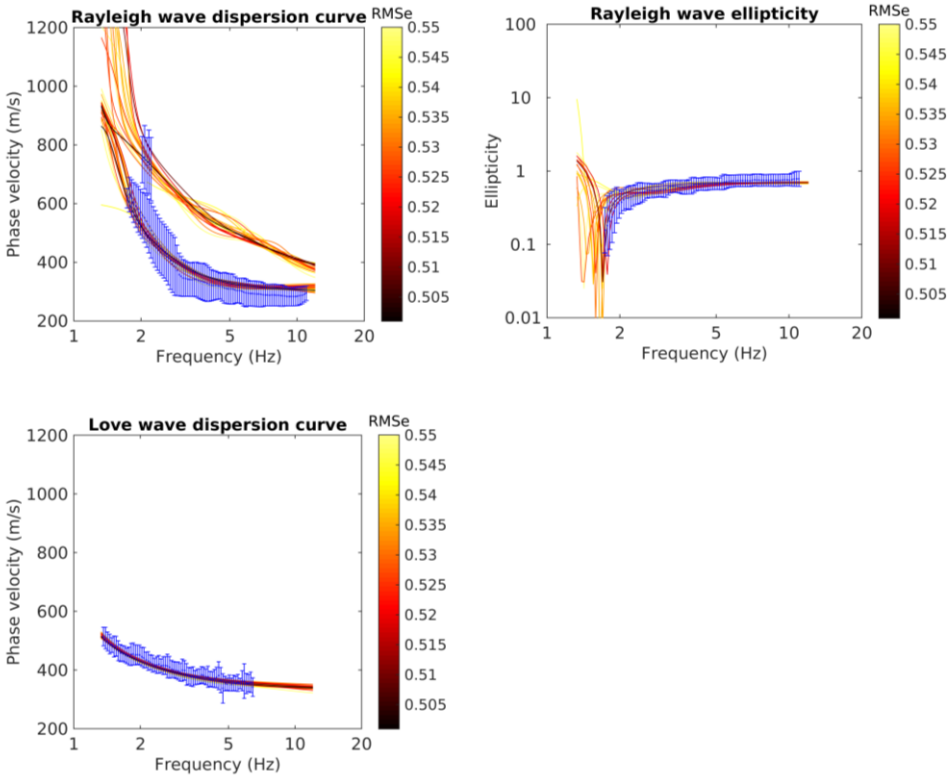

Figure 15 – 6-layer parameterization inversion: fit between experimental data (blue dots with error bars) and synthetic curves (colored lines) for the 20 best performing models.

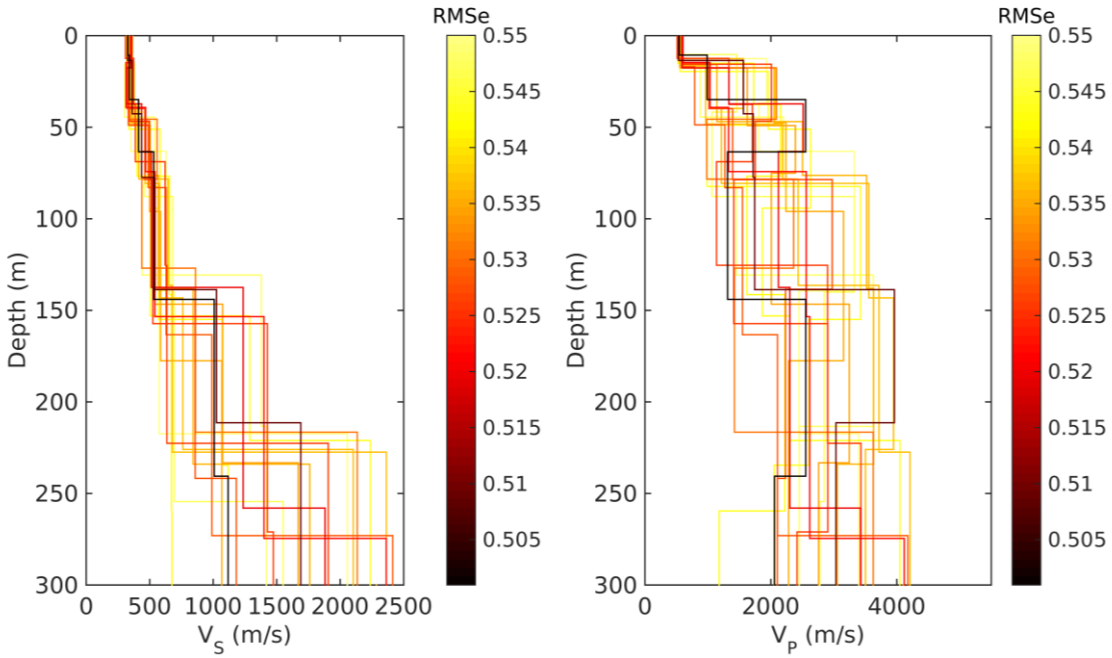

Figure 16 – 6-layer parameterization inversion: 20 best performing models.

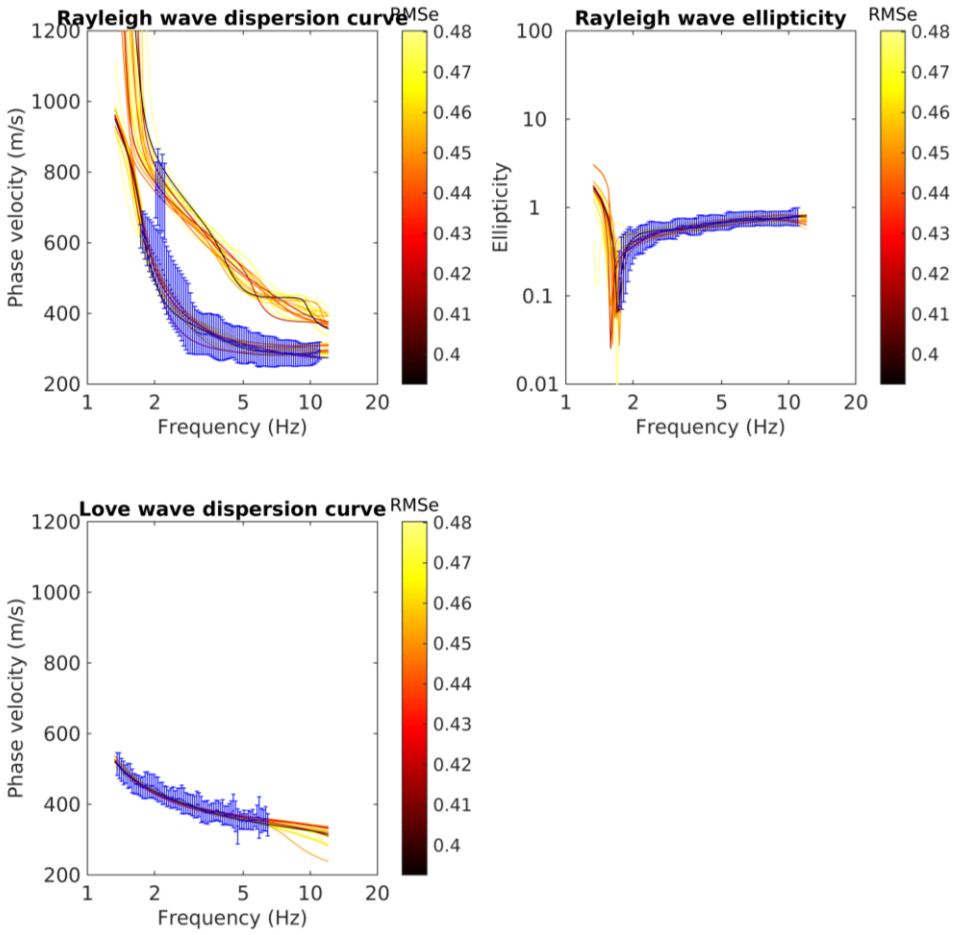

Figure 17 – 14-layer parameterization inversion: fit between experimental data (blue dots with error bars) and synthetic curves (colored lines) for the 20 best performing models.

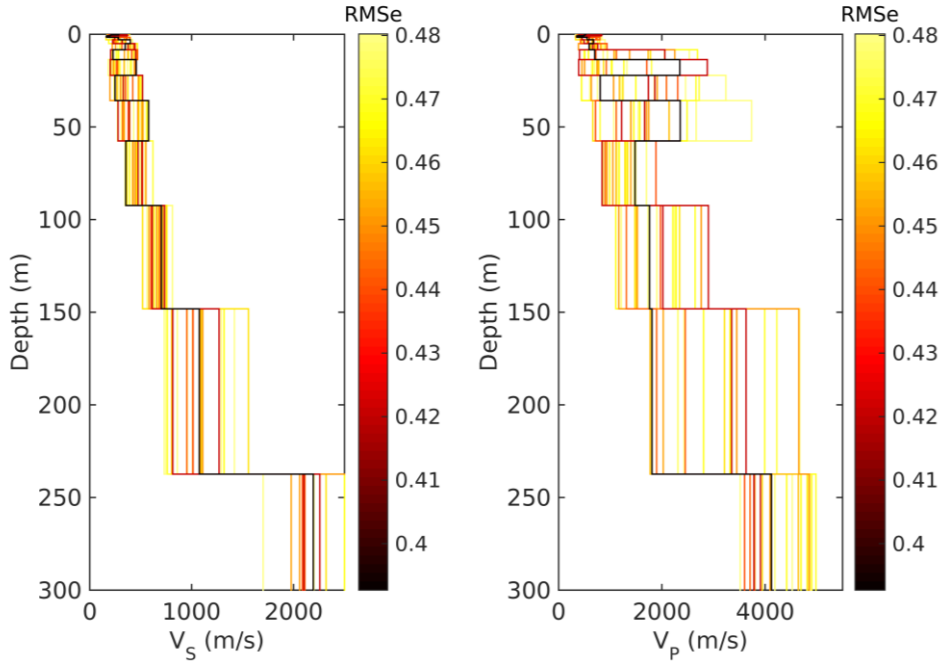

Figure 18 – 14-layer parameterization inversion: fit between experimental data (blue dots with error bars) and synthetic curves (colored lines) for the 20 best performing models.

6 Interpretation

In this section, the geological interpretation of the obtained velocity profiles (Figure 19) is discussed.

6.1 Interpretation of the velocity profiles

The final result of the inversion process is constituted by a set of 21 V_S-V_P velocity models, the best performing models from each of the three inversion runs adopting either the 6-, 7-, or 14-layer subsurface parameterization (7 models from each inversion run); these velocity profiles are represented in Figure 19, where they show a good reciprocal consistency.
The shallowest 40-50 meters have an S-wave velocity around 350 m/s and they are likely to be constituted, as per the geological atlas (Figure 2), by alluvial sediments. Below, V_S gradually increases until reaching about 650 m/s at ~150 m depth; this depth range might be occupied by sediments more compacted by self-weight, or moraine (which borders the basin where SUSI is located). The bedrock is met at approximately 150 m depth, and it has a V_S of about 1000 m/s (weathered rock). It should be noted that the Swisstopo bedrock model for Switzerland (Swisstopo, 2019) grossly underestimates the bedrock depth below SUSI (the predicted depth is 30 m).
The obtained velocity profiles show a further increase in S-wave velocity at about 250 m depth, suggesting a transition between weathered to fresh rock below; however, this interface lies at the lower boundary of the investigation depth, so it has to be accepted with a certain level of uncertainty.

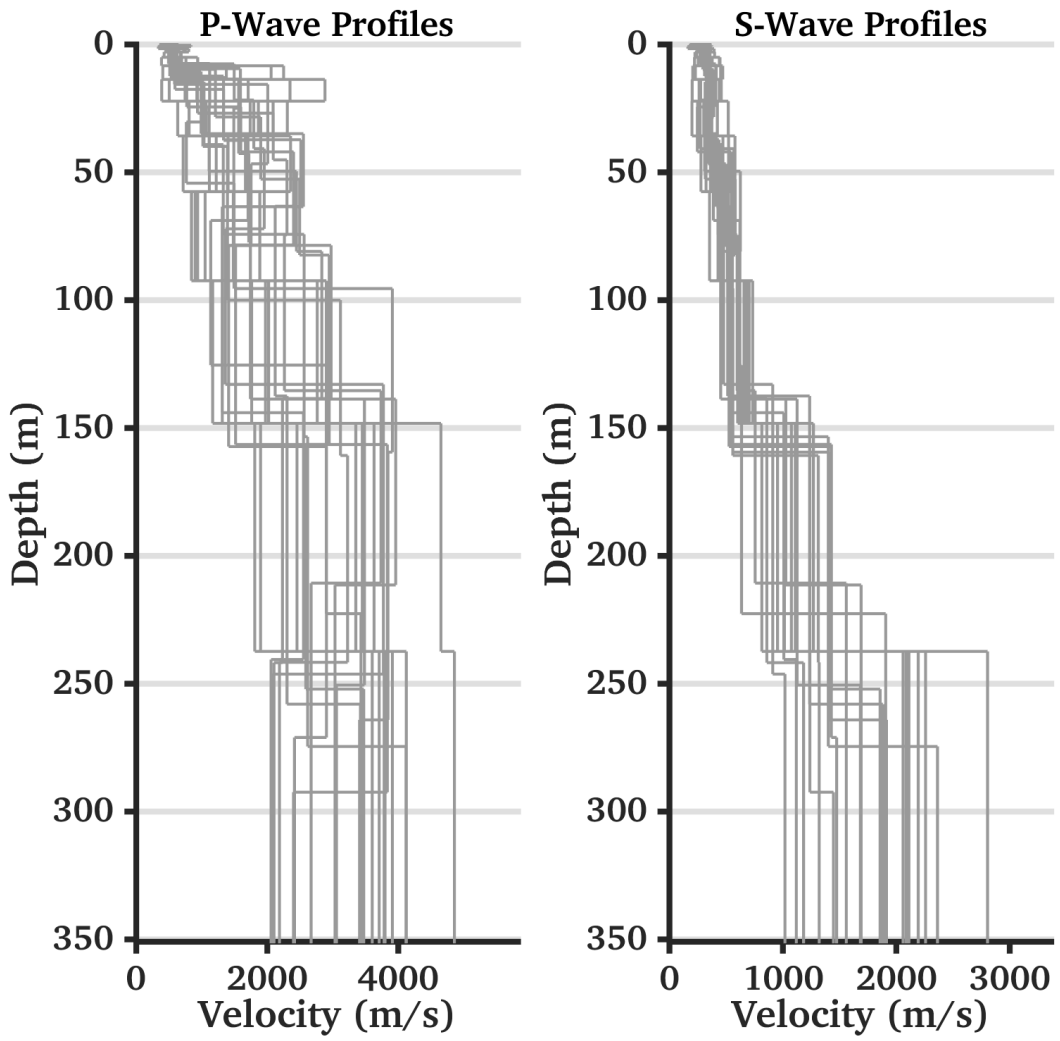

Figure 19 – 21 V_S-V_P models assumed as final inversion result. These are the 7 best performing models from each of the three inversion runs adopting either the 6-, 7-, or 14-layer subsurface parameterization.

6.2 2D Resonance

The geomorphology of the investigated area, a sedimentary basin, suggests the presence of a 2D resonance behavior for site SUSI; this is experimentally confirmed by the analyses we performed over the noise resonance frequency (Figures 5, 6) and the directionality of particle motion (Figure 9). In fact, the fundamental frequencies retrieved from the stations composing the measuring array do not show significant spatial variability, as one would expect with a concave bedrock surface in a purely 1D resonance condition; furthermore, the marked directionality of particle motion at the resonance frequency – parallel to the North-South axis of the basin – indicates a SH resonance phenomenon (Bard and Bouchon, 1985; Ermert et al., 2014).
We compared the inferred morphological and geophysical properties of the sedimentary body on which station SUSI is located with the outcomes of the numerical simulations of Bard and Bouchon (1985) on synthetic sine-shaped valley.

According to Bard and Bouchon (1985), in sediment-filled valleys 2D resonance prevails over 1D when the valley shape ratio (h/l) exceeds a critical value defined as

$$(h/l)_c = 0.65\,(C_v\text{-}1)^{1/2} \qquad (1)$$

where h is the maximum thickness of the sedimentary cover, l is the half-width of the valley (the width at $h/2$ depth) and C_v is the S-wave velocity contrast between sediments and bedrock. For the geometry of the sedimentary body, we assumed h as being equal to the depth at which the estimated S-wave velocity profiles (Figure 19) exceed a V_S of 800 m/s (approximately 150 m). As for the half-width l of the basin, we resorted to the Swisstopo (2019) bedrock model, which indicates a value of ~350 m (Figure 20). However, keeping in mind that this bedrock model largely underestimates the bedrock depth (see previous section), also the information about the basin width should be accepted with care. The values of velocity contrast C_V are derived from the profiles in Figure 19.

The resulting position of the 21 selected velocity models on the shape ratio *vs* velocity contrast plane is shown by the blue circles in Figure 21; these are located in proximity of threshold line defined by equation 1, although mostly below it (hence in the portion of the graph referring to 1D resonance and lateral propagation). Nevertheless, the experimental evidence for a 2D SH resonance phenomenon is quite compelling (Figures 5, 6, 9); therefore, it could be proposed that the width of the sedimentary body proposed by the Swisstopo (2019) bedrock model is overestimated, which could move the blues circles in Figure 21 in the upper half of the graph.

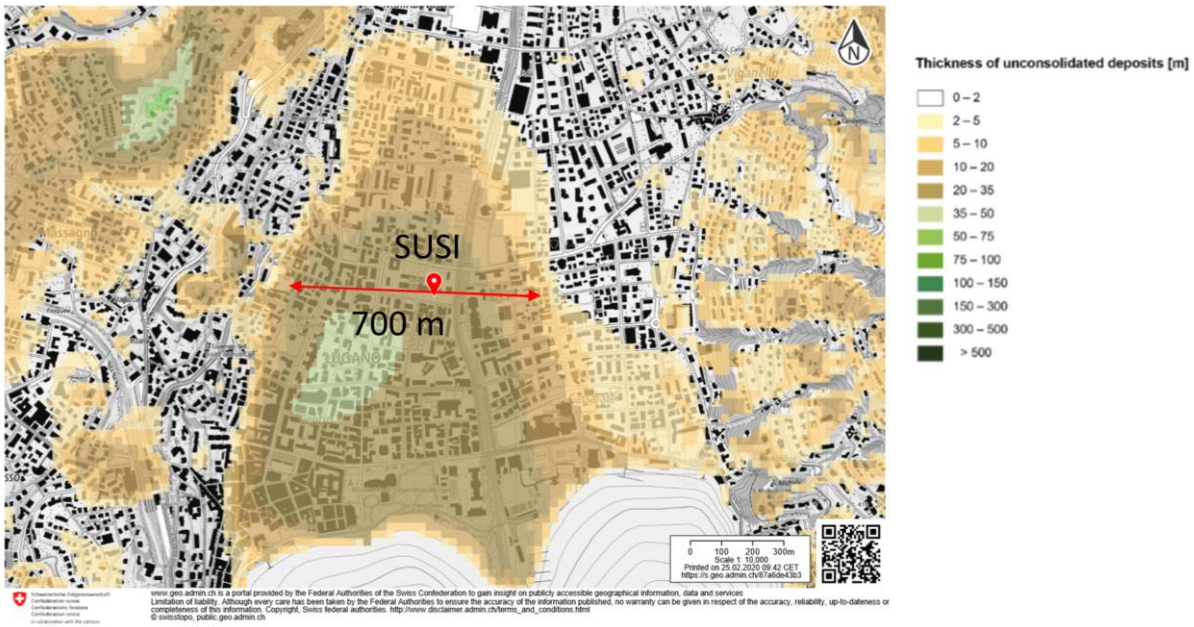

Figure 20 – Geometry of sediments in the Cassarate basin according to the bedrock model of Swisstopo (Swisstopo, 2019). The model was used to determine the width of the sedimentary body on which SUSI is located (700 m).

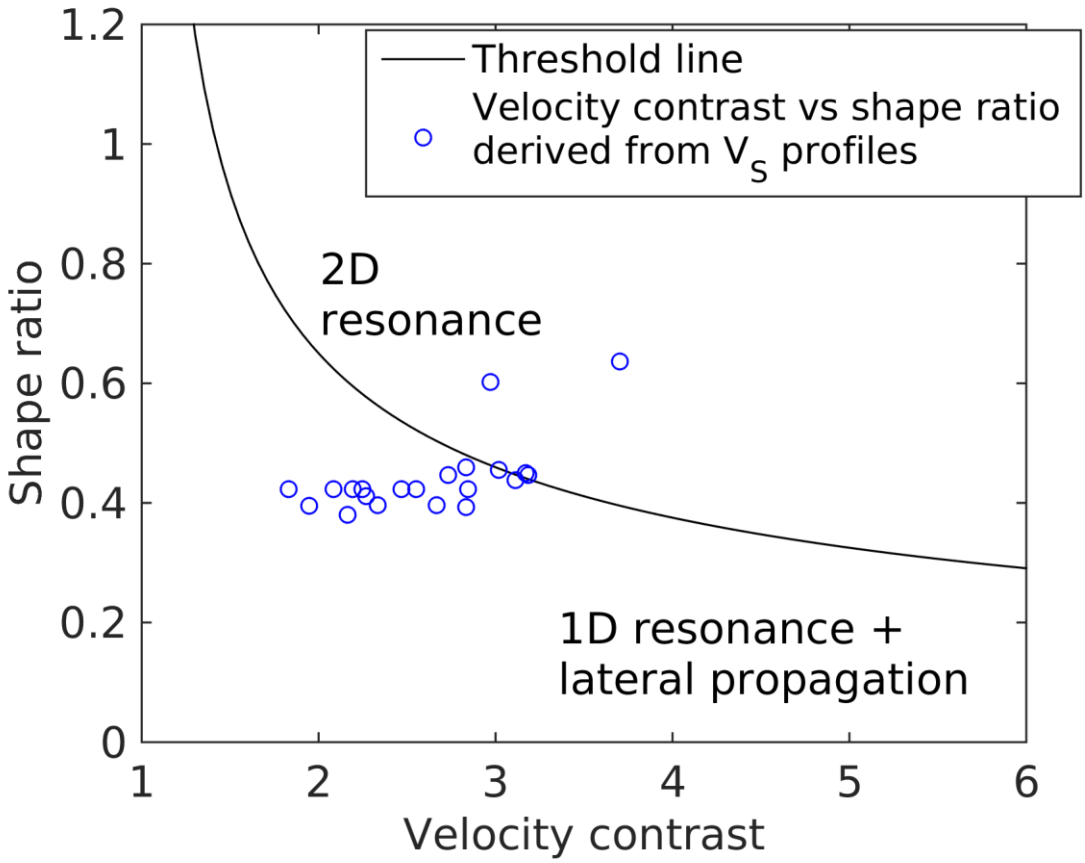

Figure 21 – Shape ratio vs velocity contrast graph (see Bard and Bouchon, 1985). Blue circles represent the h/l-Cv coordinates derived from the velocity profiles in Figure 23 (same color scale), assuming a resonant basin occupying a cosine-shaped valley bottom.

6.3 Quarter-wavelength representation

The quarter-wavelength velocity representation (V_S^{QWL}; Joyner et al., 1981) attributes the average velocity at a depth equal to ¼ of the corresponding wavelength to each frequency. V_S^{QWL} can be used as direct proxy for the local site characterization, as it physically relates the resolution on ground parameters with the characteristics of the propagating wave-field at the discrete frequencies. The derived quarter-wavelength impedance contrast (IC^{QWL}; Poggi et al., 2012) is the ratio between two quarter-wavelength average velocities from the top and bottom part of the velocity profile at a given frequency. It is a powerful tool to assess the influence of resonance phenomena in soft sediment sites.

Figure 22 shows the average (over the population of the selected 21 best subsurface models) quarter-wavelength velocity (Figure 22 centre) and impedance contrast (Figure 22 bottom) representations. The obtained Vs30 (which is the average velocity corresponding to a quarter-wavelength of 30 m) is 328 m/s.

The IC^{QWL} graph shows one peak at 0.8 Hz, which can be associated with the interface (located at approx. 150 m depth) between incoherent sediments and rock (Figure 21).

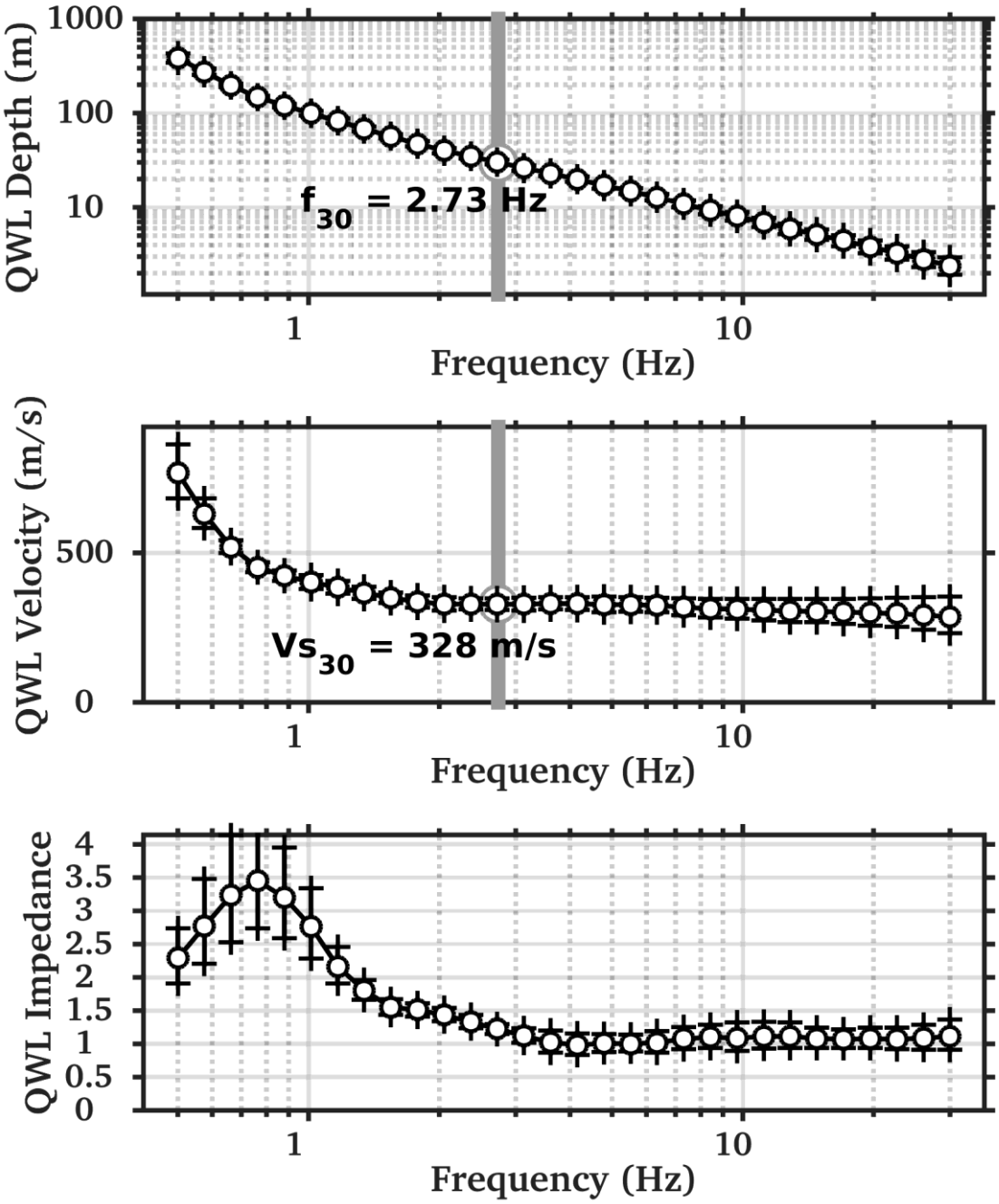

Figure 22 – Average quarter-wavelength (qwl) representations for the final profiles displayed in Figure 19. Top: qwl-depth; center: qwl-velocity; bottom: qwl-impedance contrast. The gray line in the top and center panel refers to Vs_{30}.

6.4 SH transfer function

The theoretical SH-wave transfer function for vertical propagation (Roesset, 1970) was computed for each of the selected models (Figure 19). The transfer functions were then corrected for the Swiss reference rock model (Poggi et al., 2011).

These theoretical amplification functions are averaged (blue line in Figure 23) and compared with the empirical amplification function obtained from spectral modeling (ESM; Edwards et al., 2013) of the SUSI recordings. The latter relies only on 5 events in the 0.8 – 6.5 Hz frequency band, and even fewer earthquakes at lower and higher frequencies (as of 16.02.2020).

The empirical function is characterized by a main peak centered at 0.91 Hz, with amplification factors reaching 8.5. The simulated amplification curve places this first peak at a lower frequency (0.85 Hz). The discrepancy is due to the existence of 2D resonance condition (see previous discussion), which moves the experimental fundamental frequency peak towards higher frequency (Bard and Bouchon 1985). Besides, the sharpness of the empirical amplification at the resonance frequency is another indication of a 2D effect.

The secondary peak at 2 Hz in the empirical amplification function is reproduced quite well by the synthetic curves. The peak is to be ascribed to the impedance contrast that can be observed at 40 – 50 m depth in the reconstructed velocity profiles.

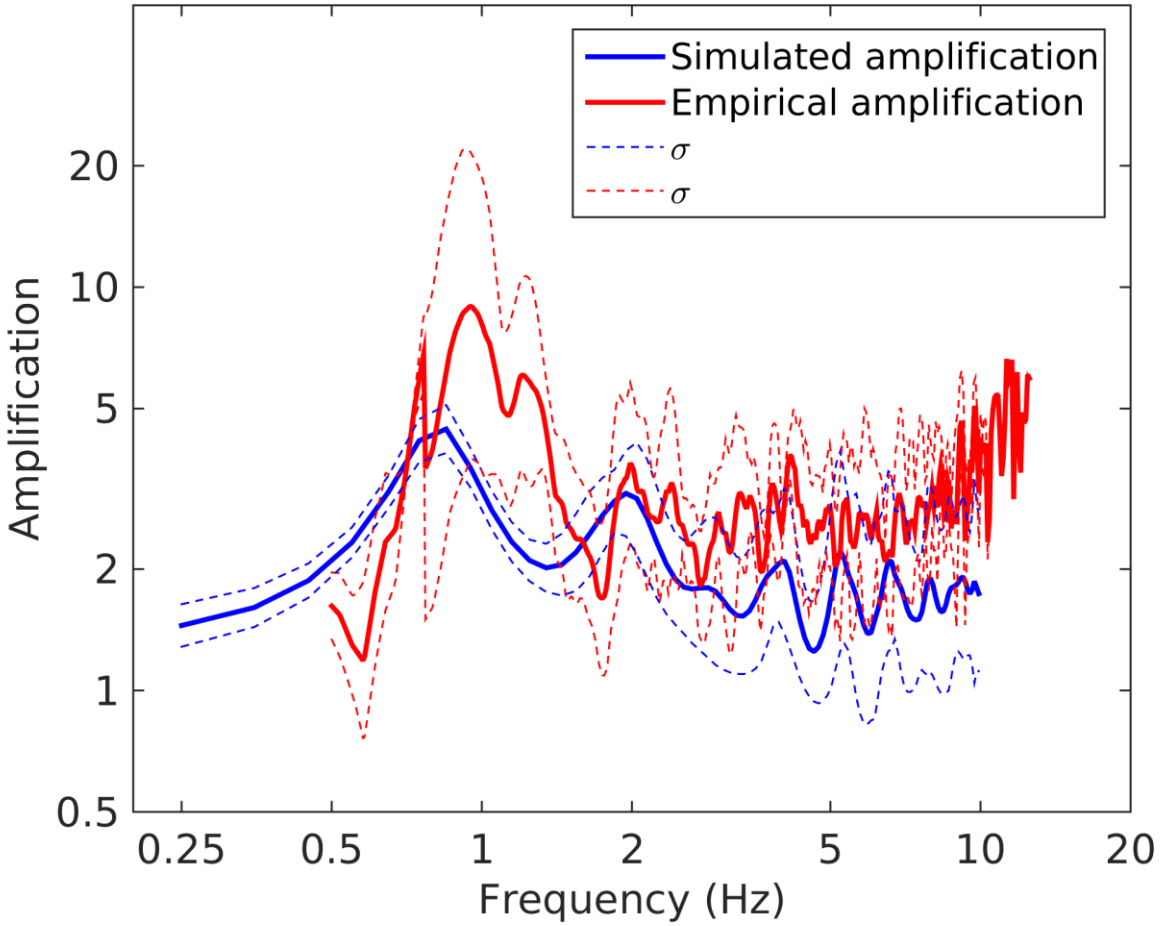

Figure 23 – Average of the modeled SH transfer functions (blue line) from the selected velocity profiles (Figure 19), corrected for the Swiss reference rock model. In red, the empirical amplification function obtained from spectral modeling.

8 Conclusions

A passive seismic survey was performed to characterize the structure of the subsurface below the SSMNet station SUSI, located in the city center of Lugano (TI), in an alluvial sediment basin.
The analysis of single-station noise recordings via H/V analysis allowed identifying the fundamental frequency of the site as 0.9 Hz; as further indicated by the polarization analysis, the peak is related to a 2D SH resonance phenomenon in the sedimentary body upon which SUSI is located.
Passive data were also processed to derive Rayleigh and Love wave phase velocity dispersion curves, and a Rayleigh wave ellipticity curve; these curves were inverted for the subsurface structure below SUSI.
The obtained geophysical model is the following: the shallowest 40-50 meters have an S-wave velocity around 350 m/s and they are likely to be constituted by alluvial sediments. Below, V_S gradually increases until reaching about 650 m/s at ~150 m depth; this depth range might be occupied by sediments more compacted by self-weight, or moraine (which borders the basin where SUSI is located). The bedrock is met at approximately 150 m depth, and it has a V_S of about 1000 m/s (weathered rock). The obtained velocity profiles show a further increase in S-wave velocity at about 250 m depth, suggesting a transition between weathered to fresh rock below; however, this interface lies at the lower boundary of the investigation depth, so it must be accepted with a certain level of uncertainty.
The obtained V_{S30} is 328 m/s (standard deviation 18 m/s); H_{800} (depth where V_S exceeds 800 m/s) is 154 m (standard deviation = 22 m); therefore, the site can be classified as type C according to both Eurocode 8 (CEN, 2004) and SIA261 (SIA, 2014).

References

BAFU (Federal Office for the environment), 2017. NACQUA-QUANT Monitoring sites data.

Bard, P.-Y., and M. Bouchon, 1985. The two-dimensional resonance of sediment-filled valleys, Bull. Seismol. Soc. Am. 75, no. 2, 519–541.

Burjanek, J., J.R. Moore, F.X. Yugsi Molina, and Donat Fäh, 2012. Instrumental evidence of normal mode rock slope vibration. GJI, 188, 559-569.

CEN, 2004. Eurocode 8: Design of structures for earthquake resistance – Part 1: general rules, seismic actions and rules for buildings. European Committee for Standardization, en 1998-1 edition.

Edwards, B., Michel, C., Poggi, V., and Fäh, D. , 2013. Determination of Site Amplification from Regional Seismicity : Application to the Swiss National Seismic Networks. Seismological Research Letters, 84(4).

Ermert L., V. Poggi, J. Burjanek, and D. Fäh, 2014, Fundamental and higher tow-dimensional resonance modes of an alpine valley. GJI, vol. 198, no. 2, pp 795-811.

Fäh, D., F. Kind, and D. Giardini, 2001. A theoretical investigation of average H/V ratios. GJI, 145, no. 2, 535-549.

Herrmann, R. B. (2013) Computer programs in seismology: An evolving tool for instruction and research, *Seism. Res. Lettr.* **84**, 1081-1088

Hobiger, M., P.-Y. Bard, C. Cornou, and N. Le Bihan, 2009. Single station determination of Rayleigh wave ellipticity by using the random decrement technique (Raydec). GRL, 36, L14303

Joyner, W. B., Warrick, R. E., and Fumal, T. E., 1981. The effect of Quaternary alluvium on strong ground motion in the Coyote Lake, California, earthquake of 1979. Bulletin of the Seismological Society of America, 71(4):1333–1349.

Maranò, S., C. Reller, H.A. Loeliger, and D. Fäh, 2012. Seismic waves estimation and wavefield decomposition: application to ambient vibrations. GJI, 191, 175-188

Poggi, V., Edwards, B., and Fäh, D., 2011. Derivation of a Reference Shear-Wave Velocity Model from Empirical Site Amplification. Bulletin of the Seismological Society of America, 101(1):258–274.

Poggi, V., B. Edwards and D. Fäh, 2012. The quarter-wavelength average velocity: a review of some past and recent application developments. 15th WCEE, Lisbon 2012

Poggi, V., and D. Fäh, 2010. Estimating Rayleigh wave particle motion from three component array analysis of ambient vibrations. GJI, 180, no. 1, 251-267.

Roesset, J., 1970. Fundamentals of soil amplification. In: Hansen, R. J., editor, Seismic Design for Nuclear Power Plants, pages 183–244. M.I.T. Press, Cambridge, Mass.

SIA, 2014. SIA 261 Einwirkungen auf Tragwerke. Société Suisse des ingénieurs at des architectes, Zurich, Switzerland.

Swisstopo, 1976. 1:25000 Geological Atlas, LK 1353 (Lugano)

Swisstopo, 2019. Thickness model of unconsolidated deposits.